Photoinduced Dislocation Lines on the (111) Face of C_{60} Single Crystals

L. Jiang,[†] T. Iyoda,[†] D. A. Tryk,[‡] J. Li,[‡] K. Kitazawa,[‡] A. Fujishima,*[,†,‡] and K. Hashimoto*[,†,§]

Kanagawa Academy of Science and Technology, KAST Laboratory, 1583 Iiyama, Atsugi-shi, Kanagawa, Japan, Department of Applied Chemistry, Faculty of Engineering, University of Tokyo, Hongo, Bunkyo-ku, Tokyo 113, Japan, and Research Center for Advanced Science and Technology, University of Tokyo, Komaba, Meguro-ku, Tokyo 153, Japan

Received: December 29, 1997; In Final Form: March 10, 1998

We report an atomic force microscopic (AFM) study of photoinduced dislocation lines (DLs) on the (111) face of C_{60} single crystals via excitation of the Frenkel exciton transition of solid C_{60}. Under illumination, DLs appeared along the [11$\bar{2}$] direction on the (111) face of the C_{60} single crystals. These DLs consist of pairs of substructures that are separated by a hollow region with a width of 30.0 ± 0.5 nm and a depth of 0.08 ± 0.02 nm, while the height difference between the topmost regions of the substructures and the surrounding face-centered-cubic (fcc) regions is 0.30 ± 0.03 nm. The two substructures correspond to ridge-like domain walls enclosing narrow strips of metastable hexagonal-close-packed (hcp) domains on the surrounding fcc surface. It was also observed that the pair of substructures constituting the DLs is terminated by a U-shaped growing tip. The photodriven growth of these DLs displayed unique dynamic surface reconstruction behavior. They also exhibited different types of collision processes depending on the growth rate. The driving force for the dynamic process is considered to be the recombination of excitons at surface defects or at the growing tip of each DL. Furthermore, a threshold light intensity value of 0.8 mW/mm^2 was found for the generation of DLs, which indicates that multiexciton relaxation is a prerequisite for the photoinduced dislocation.

1. Introduction

Surface reconstructions have been widely studied on metals and semiconductors.[1] Much of this work has focused on the critical behavior of incipient surface reconstruction, for example, by means of low-energy electron diffraction (LEED),[2] transmission electron microscopy (TEM),[3,4] scanning tunneling microscopy (STM),[5,7] and atomic force microscopy (AFM).[8,9] Generally, surface reconstruction results from the relaxation of the atoms or molecules in the outermost layer of a surface away from their ideal bulk positions. In a certain parameter range, their positions are usually minimal in energy and appear to constitute a metastable structure. These surface structures have been generated and modified by different types of stimulation. The surface reconstruction can be created by thermal treatment, e.g., on the surface of Au(111).[3,5] Reversible surface reconstruction can be controlled in an electrochemical system by applying redox potentials, e.g., on the surface of Ag(111) and Au(111).[10] The surface reconstruction can also be induced by introducing adsorbates on a clean surface, e.g., the CO/Rh(110), Cu/Ru(0001), and Ag/Pt(111) systems.[11−14] Thus far, no photoinduced surface reconstruction has been reported.

Photoinduced phase transitions have been investigated in several types of organic crystals.[15−17] However, no direct observation of the structural changes has been reported. The microscopic structural changes are only vaguely understood, and the dynamic processes of the phase transition are still unclear. Considering the light penetration depth in these solids, the photoinduced structural transformations may occur only on the surface or in the near-surface region. Moreover, from the viewpoint of the activation energy, the structural transformation is more easily induced on the surface than in the bulk of the solid. Scanning probe techniques appear to have much potential for the direct imaging of the dynamic process of surface structural transformations on the microscopic scale.[18−20] Recently, we have studied the photoisomerization processes on the surface of azobenzene single crystals[21] and interfacial photochemical reactions on the surface of TiO_2 single crystals by AFM and friction force microscopy (FFM).[22,23] In the present work, we report, for the first time, the direct observation of the dynamic process of a photodriven reconstruction on the surfaces of C_{60} single crystals which were imaged in situ in real time by use of AFM.

Surface structural properties of fullerenes have been extensively studied on thin films supported by different types of substrates (e.g., metals, semiconductors, and alkali halides), where various molecular arrangements were observed.[24,25] For example, a stressed commensurate monolayer was found on the surface of the C_{60}/Au(100) system by STM.[26] Overlayer growth was observed on the surface of the C_{60}/GaAs(110) system at room temperature by STM, which appears as a dislocation array along the [11$\bar{2}$] direction.[27,28] Two surface phases ($3\sqrt{3} \times 3\sqrt{3})R30°$ and $(\sqrt{13} \times \sqrt{13})R14°$ as well as a localized metastable 5×5 phase were identified by LEED and STM on the surface of a molecular monolayer in the C_{60}/Ge(111) system.[29] A periodic dislocation array was found along the [110] direction on the surface of the C_{60}/GaAs system at 450 K by STM,[30,31] which was further understood as the coexistence of two domain structures by LEED observation.[32] Similar surface structures[33] and screw dislocations[34] were also observed

* Corresponding authors.
† Kanagawa Academy of Science and Technology.
‡ Department of Applied Chemistry, University of Tokyo.
§ Research Center for Advanced Science and Technology, University of Tokyo.

S1089-5647(98)00588-4 CCC: $15.00
Published on Web 07/25/1998

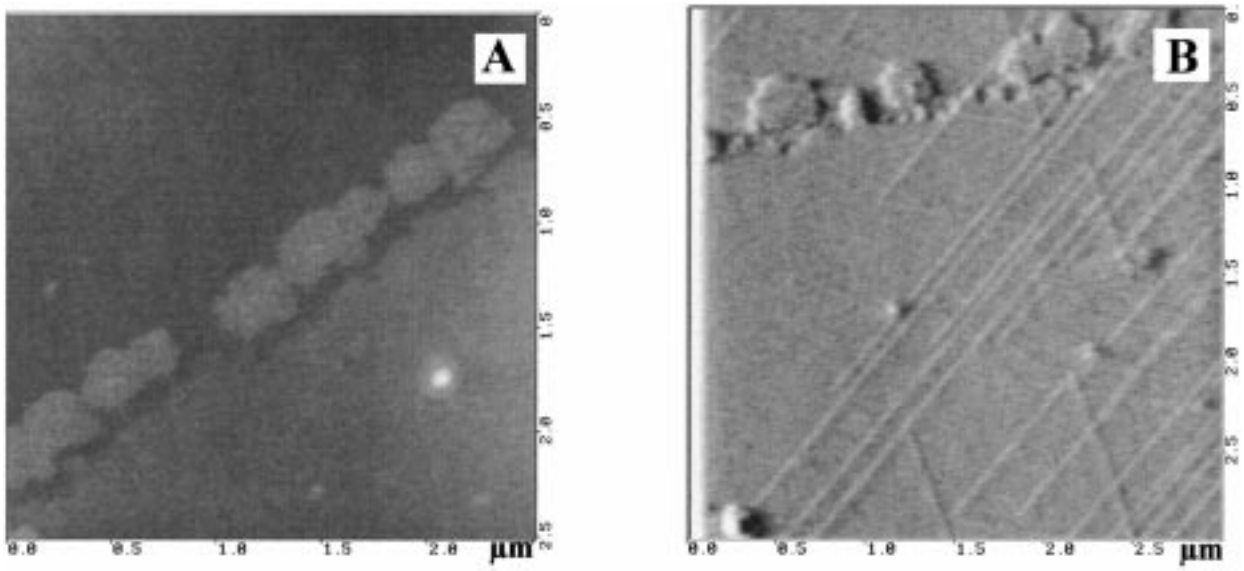

Figure 1. AFM images of surface structure of the (111) surface of C_{60} single crystals, (A) before illumination (constant height mode image) and (B) after illumination.

on the surface of the C_{60}/KBr(001) system by AFM. However, a pure surface reconstruction, i.e., one not involving the influence of a substrate, has been observed only on the (0001) face of C_{70} single crystals.[35−37] This reconstruction occurs as a long-range periodic array of dislocation lines consisting of ridged domain walls between face-centered-cubic (fcc) and hexagonal-close-packed (hcp) stacking regions. The reconstruction is consistent with the small cohesive-energy difference between the fcc and hcp phases ($\Delta E = 0.34$ kcal/mol), hcp being more stable at room temperature.[38] We also predicted that there should be a similar surface reconstruction on the C_{60} single crystal,[36] for which ΔE has been estimated to be 0.90 kcal/mol, with the fcc phase being more stable.[36] In the present work, we undertook the induction of this surface reconstruction by optical stimulation.

The general strategy for exploring photoinduced surface reconstruction systems is as follows: (I) to search for a metastable surface phase that may be induced by a photophysical process, in which the energy difference between the stable and metastable phases is relatively small and the barrier between the two phases is relatively high; this may allow the existence of the metastable phase or may allow the coexistence of the two states (or phases) in local areas of the solid surface; (II) to select the excitation within the Urbach tail[39,40] of the lowest exciton absorption band, where strong electron−lattice coupling is expected. For a suitable system, the electron−lattice coupling constant (g) should be greater than 1.[40] These prerequisites are met in the case of C_{60}. As mentioned above, it has a metastable hcp phase, and the cohesive-energy difference between the hcp and fcc phases is indeed small. Moreover, the electron−lattice coupling constant g for the C_{60} single crystal is reported to be about 3.7,[41] which is much larger than that for the other typical molecular systems.[40] Therefore, the C_{60} single crystal is a good candidate for the exhibition of a photoinduced surface reconstruction. Although studies have been reported on photoinduced surface modifications of C_{60} solid via super-band gap illumination,[42,43] these changes were based on photochemical reactions. The present photoinduced reconstruction is, however, induced by sub-band gap excitation, i.e., the lowest exciton absorption of solid C_{60}. The surface molecular rearrangement is expected to be induced via photophysical processes.

2. Experimental Section

C_{60} single crystals were prepared using an improved descending-temperature vapor-phase transport method.[44] Chromatographically purified C_{60} powder was placed at one end of a long sealed silica ampule under vacuum. The ampule was placed in a horizontal furnace, where the temperatures at the two ends of the ampule, T_s (source) and T_c (crystal), were controlled independently to adjust the supersaturation ($\Delta T = T_s - T_c$). Large single crystals, with dimensions of several millimeters, can be grown by this technique. High-quality crystals could be obtained when the temperatures were programmed at $T_c =$ 542 °C and $T_s = 550$ °C ($\Delta T = 8$ °C), with T_c descending at a rate of about 5 °C/day, while T_s was kept constant at 550 °C. X-ray diffraction measurements indicated that the crystals exhibited the fcc structure.

As-grown C_{60}(111) crystal surfaces were imaged by use of AFM in the dark and under illumination. Similar results were obtained at a number of different sites on several crystals. AFM measurements were carried out with a Seiko model SPA 3700 instrument under ambient conditions. A triangular-shaped Si_3N_4 cantilever with a spring constant of 0.02 N/m was used to acquire images in the contact mode. The applied force was typically 0.1 nN. Under the above imaging conditions, no surface modification effects were observed during the imaging process. Except as mentioned, the images in the present work were obtained in the constant height mode, while precise height information was obtained from simultaneous constant force mode images. Considering that photopolymerization occurs in solid C_{60} under illumination with super-band gap photon energies (>2.3 eV),[45,46] we used a semiconductor laser with a wavelength of 670 nm (1.85 eV) and power of 50 μW as a light source to induce the lowest exciton absorption in the 1.5∼2.0 eV region.[47] The light intensities were varied either by using a neutral density filter or by adjusting the diameter of the laser beam.

3. Results and Discussion

The as-grown (111) face of C_{60} single crystal was imaged with AFM, one of the images being shown in Figure 1A. In the image, a step structure and small nuclei are observed on a molecularly flat surface of the crystal. The height of the step

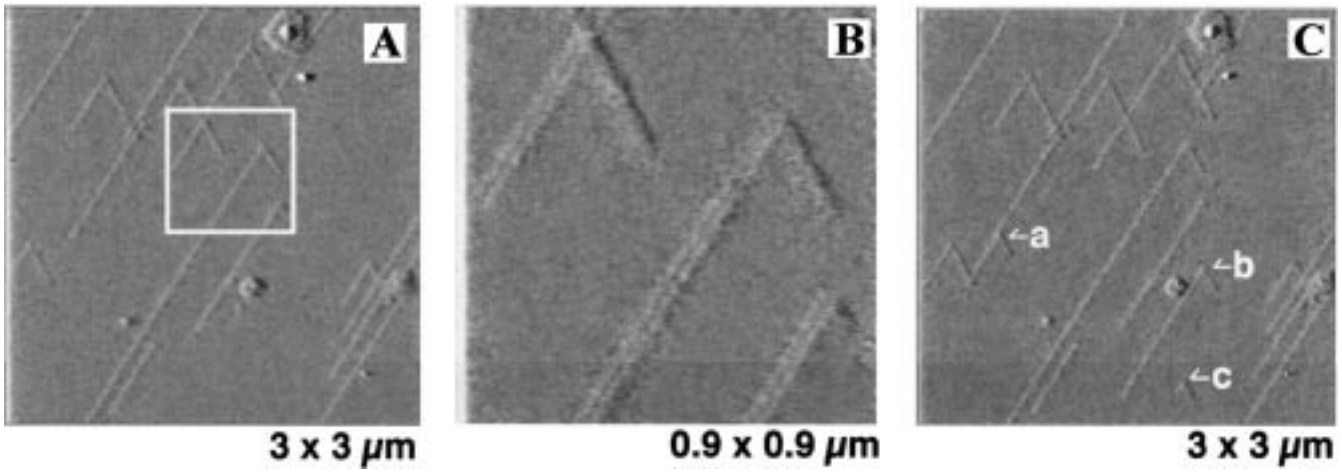

Figure 2. (A) AFM image of the initial states of photoinduced surface reconstruction, (B) a zoomed-in image of image A, and (C) an image of the same area of image A after 20 min of illumination.

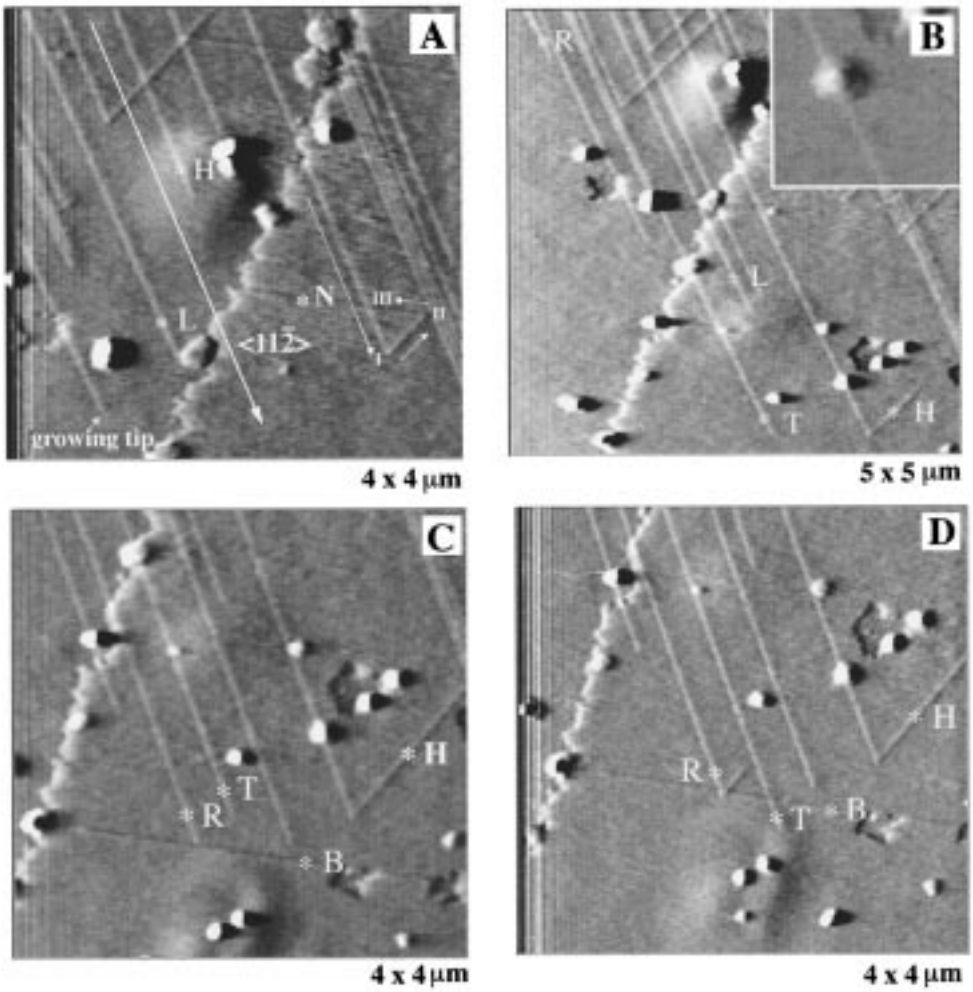

Figure 3. Sequential AFM images of the propagation and collision processes of dislocation lines (DLs) under laser illumination at an intensity of ~1.4 mW/mm^2. Image (A) was obtained after 30 min of preillumination. Images (B), (C), and (D) were acquired 5, 15, and 17 min, respectively, after obtaining image (A). The inset in image (B) shows a DL that has passed through a two-layer island without change in structure and direction. The DLs show various growth rates during the growth process; for example, DL H (high growth rate type) grows faster than DL L (low growth rate type). In images (C) and (D), DL R (reflection type) and DL T (transmission type) show different types of collision behavior after colliding with DL B.

is 0.98 ± 0.3 nm, which corresponds to the thickness of a monolayer of C_{60} molecules. During the imaging process, repeated scanning over the same sample area of the surface produced no changes in the images, thus indicating that tip-induced modification was negligible. Under illumination with an intensity of ca. 1.1 mW/mm^2 for 30 min, dislocation lines (DLs) were observed along the [112] direction, as shown in Figure 1B. These DLs could be generated even in an ultrahigh-vacuum condition (3×10^{-10} Torr) when the illumination was performed. This implies that the photoinduced surface recon-

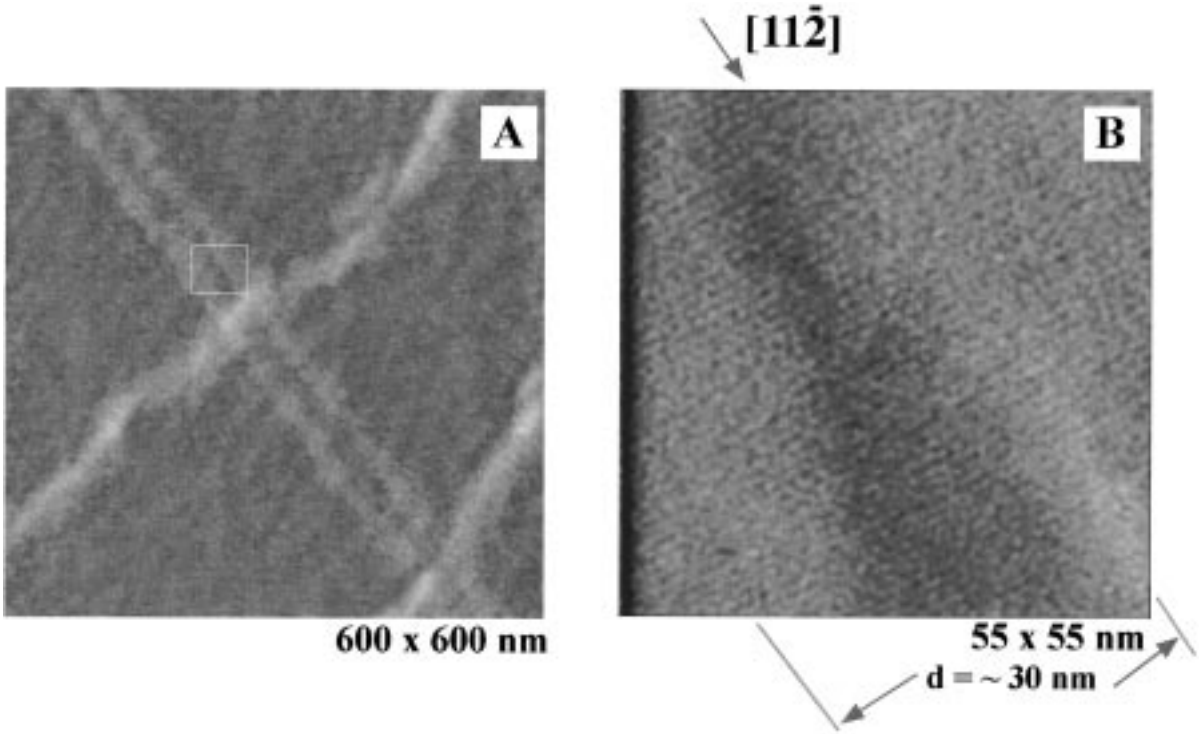

Figure 4. (A) Zoomed-in AFM image of the DL and (B) molecular resolution image.

struction is not influenced strongly by possible gas-phase adsorbates such as oxygen.

Light intensity dependence studies indicated a threshold value of ca. 0.8 mW/mm^2 for the photoinduced surface reconstruction. Under illumination with a nearly threshold intensity, the initial state of reconstruction was observed as shown in Figure 2. In Figure 2A, several DLs are distributed on the surface. These DLs begin propagating from particular initiation points on the surface and grow in one or two equivalent [11$\bar{2}$] directions away from the center of the laser spot. (Note: in every image, the center of the laser beam is near the top part of the image.) The zoomed-in image (Figure 2B) shows that each DL consists of two substructures. After further illumination for 20 min, new DLs were induced from three initial points, as labeled by a, b, c in Figure 2C, while the other DLs did not change. These initial reconstruction points were found to be distributed randomly on the surface. The observations suggest that the DLs start only at special points, which are probably molecular level defects on the surface of the crystal.

By increasing the light intensity (e.g., 1.4 mW/mm^2), one can also observe the photodriven motion of the DLs by imaging the surface during illumination. The DLs with the growing tip (as labeled in Figure 3A) were observed near a monolayer step edge. Figure 3A was obtained after 30 min illumination. Figure 3 (A−D) shows a series of AFM images obtained during illumination. The dynamic reconstruction process can be recognized by the motion of the growing tips of individual DLs in the images. Careful comparison of parts A and B Figure 3 indicates that the reconstruction proceeds at various growth rates, e.g., DL H grows faster than DL L. Moreover, DL H changes its growth direction by 120° in the counterclockwise (CCW) direction with respect to the original [11$\bar{2}$] direction. However, during all of these propagation processes, the cross-sectional DL structures are perfectly maintained.

Another interesting feature is the collision behavior of these structures. Figure 3C,D shows images obtained before and after DLs R and T collide with B. Two types of collision processes are observed: (i) DL R changes direction CCW by 120°, and (ii) DL T passes through DL B with no change in growth direction. Recalling the growth history of these DLs in Figure 3B,C, it is obvious that DL R grew at a much faster rate than DL T. This suggests that the growth rate has a certain relationship with the dynamic reconstruction process. By analyzing the dynamic behavior of more than 30 DLs, the propagation processes can be roughly classified into three types,[48] in decreasing order of average growth rate $\nu_{\langle 11\bar{2}\rangle}$: type I ($>\sim$20 nm/s), in which DLs change direction without collision (e.g., H); type II (20 nm/s $> \nu_{\langle 11\bar{2}\rangle} >$ 3 nm/s), in which DLs change direction after colliding with other DLs (e.g., R); and type III ($\nu_{\langle 11\bar{2}\rangle} < \sim$3 nm/s), in which DLs continue to grow or pass through other DLs even after colliding with them (e.g., T). It is sometimes observed that all of the processes mentioned above can appear in a single DL. For example, the triangular trace of DL N (Figure 3A) exhibits spontaneous turning, collision-induced turning, and self-intersection, indicating that the DLs reduced their growth rate after changing direction. It should be noted that the DLs can also pass through monolayer steps (Figure 3B), surface nuclei (inset of Figure 3B), or other DLs (Figure 3D) without dissipating. The dynamic process responsible for the surface reconstruction described here can be theoretically described using the concept of a solitary wave (double-sine-Gordon soliton).[49] This concept has been applied in describing inorganic systems such as the Au(111) surface.[50]

A zoomed-in image (Figure 4A) shows the detailed structure of a DL. A DL, with its pair of substructures, was observed on two monolayer steps. The molecular resolution image (Figure 4B) shows the molecular arrangement in the DL at the highest magnification achievable under the present imaging conditions. Although the molecular arrangement is slightly disordered due to the tip modification effect (relatively high scanning rate was used during the molecular resolution imaging process), the hexagonal molecular arrangement is still distinguishable in local areas of the image. According to these molecular arrangements, the orientational direction of the DL

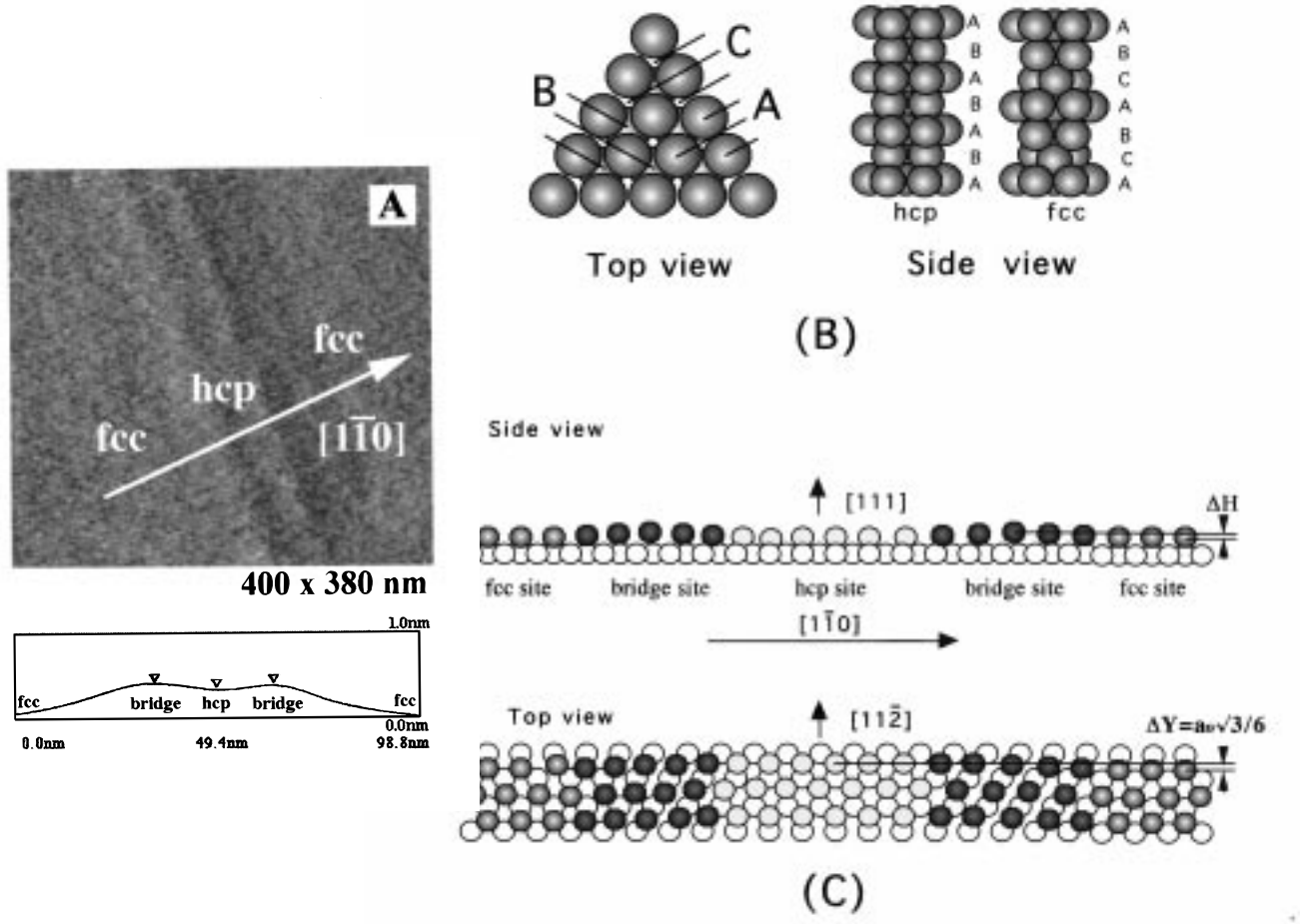

Figure 5. (A) AFM image of a DL with two substructures. The lower part of the image shows a cross section of the image scanned between A and B along the $\langle 1\bar{1}0\rangle$ direction. (B) Molecular stacking of the fcc and hcp structures. (C) Molecular arrangement model of the top two layers of molecules comprising the pair of substructures in a DL along the [1$\bar{1}$0] direction. The top view is projected along the [111] direction, and the side view is projected along the [11$\bar{2}$] direction. The number of molecules involved in the dislocation (ridge to ridge) has been decreased from ~30 to ~12 for clarity. The highest elevation molecules, i.e., those forming the domain walls, are represented as filled circles, and those occupying the various types of sites (fcc, bridge, hcp) are represented by different colors. The second layer molecules are shown as open circles.

can be understood at the molecular level, i.e., the DLs run parallel to the $\langle 11\bar{2}\rangle$ direction, and the molecular arrangement in the dislocation region is essentially hexagonal. The profile obtained along the $\langle 1\bar{1}0\rangle$ direction of a substructure pair in Figure 5A (lower part) indicates that the two substructures are separated by a hollow region with a width of 30.0 ± 0.5 nm and a depth of 0.08 ± 0.02 nm, while the height difference between the topmost region of the substructure and the surrounding fcc region is 0.30 ± 0.03 nm (as shown in Figure 5A). The hollow region between the two ridged substructures is so shallow that the two substructures can be distinguished only at relatively high magnification.

These observations of the reconstruction allow us to infer a fcc−hcp stacking transition on the C_{60} single-crystal surface. As already mentioned, there are two possible arrangements, the hcp and fcc structures, for the C_{60} single crystal. In both cases, the planes of highest molecular density, (0001) and (111), have the same in-plane hexagonal molecular arrangement. However, the sequences of consecutive planes forming the bulk stacking structure are different: in the case of hcp, the molecules of every second layer occupy one of the three (every second out of six) concavities, e.g., B in Figure 5B (top view), around each molecule, A, while the molecules of every consecutive odd layer are positioned exactly above the molecules in the first layer, giving rise to an ABAB... sequence of planes and to a hcp bulk structure in Figure 5B (side view). In the case of fcc, every third consecutive layer occupies a concavity lying above a concavity in the first layer. Therefore, an ABCABC... sequence of planes results, forming a fcc bulk lattice. The most stable phase for C_{60} at room temperature is fcc, which is favored by 0.90 kcal/mol versus the hcp phase.[38] This small cohesive-energy difference provides the possibility for the local coexistence of the two phases on the C_{60}(111) surface, which has indeed been observed on the surface of C_{60} thin films.[51] As mentioned above, hcp and fcc stackings appear in different planes in the bulk of the crystal. On the surface of the crystal, these two stacking forms may coexist in the same topmost layer through a stacking transition from fcc sites to hcp sites or vice versa. However, this transition is not an isotropic one; similar to the Au(111) surface or other fcc systems,[5] the minimum-energy path for this transition is in three equivalent [1$\bar{1}$0] directions. The hcp domains grow in one-dimensional form along the [11$\bar{2}$] directions. Moreover, the hcp domain and surrounding fcc regions are not connected directly to each other but are separated by two ridged domain walls.

The total width of the pair of substructures extends over about 90 nm, which corresponds to nearly 100 C_{60} molecules in the $\langle 1\bar{1}0\rangle$ direction (Figure 5A). Figure 5C shows a model of the detailed molecular arrangement in a DL with a pair of domain walls. To occupy the fcc sites and hcp sites in the same layer, the molecules gradually shift position along the [1$\bar{1}$0] direction from fcc sites to hcp sites through bridge sites (domain wall region) and return to fcc sites through other bridge sites (Figure 5C, top view), which appears as a $\sim 90 \times \sqrt{3}$ unit cell. This

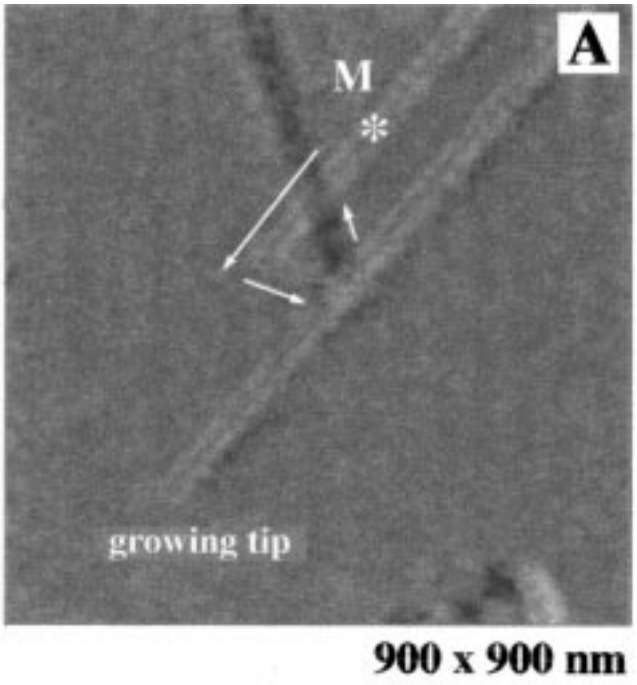

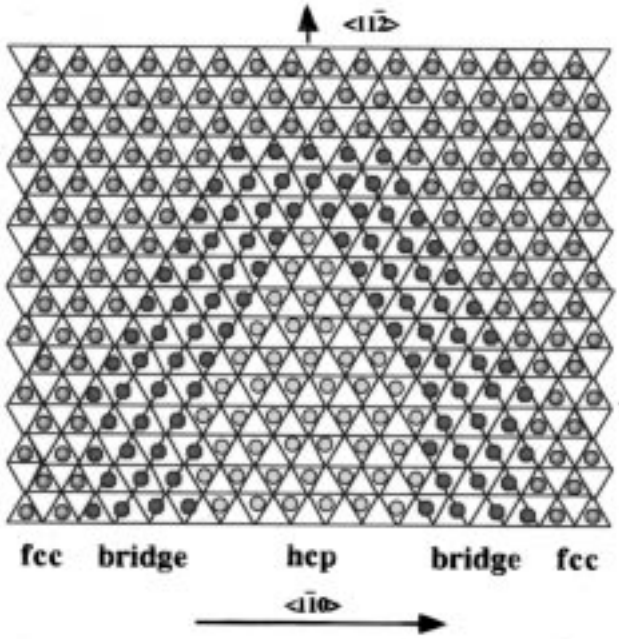

Figure 6. (A) AFM image of the reconstructed surface, showing the presence of two substructures in two DLs. The growing tip shows a U-shaped termination. DL M exhibited a growth trace similar to that of DL N (in Figure 3A). (B) U-shaped molecular arrangement model of the growing tip, indicating that the pair of substructures are connected to each other. The layer underlying the very top layer is represented by the triangular network, with molecules at each intersection, and the top layer is represented by the filled circles. As in Figure 4C, the number of molecules involved in the dislocation region has also been decreased for clarify.

unit cell is much larger than that of Au(111), which is $\sim 23 \times \sqrt{3}$. On the other hand, the partial molecular dislocation from fcc to hcp sites in the [1$\bar{1}$0] direction also results in a total dislocation in the hcp region along the [11$\bar{2}$] direction, designated as Δy (Figure 5C, top view). In the bridge sites, the positions of the molecules are also raised gradually along the [111] direction (Figure 5C side view, where the height

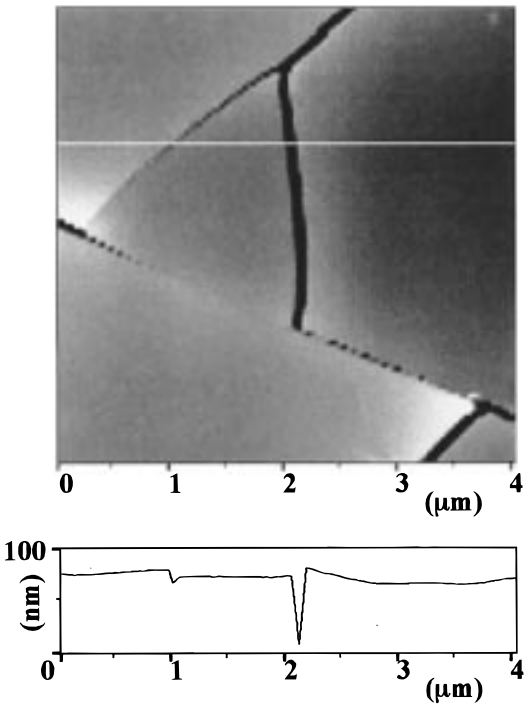

Figure 7. (A) Typical AFM image of a cracked surface [C_{60}(111)] which was generated by super-band gap illumination, with a photon energy of 2.41 eV. (B) Profile of the image.

change is denoted as Δz), and thus they appear higher in the AFM images. Therefore, the reconstruction is manifested by cooperative dislocations in the [11$\bar{2}$], [1$\bar{1}$0], and [111] directions.

It was also found that the pair of substructures contact each other at the growing tip and form a U-shaped termination, as shown in Figure 6A. In fact, similar U-shaped structures have also been reported on Cu/Ru(0001),[18] Pt(111),[52] and Au(111).[53] Accordingly, the molecular arrangement of the growing tip is proposed to be as shown in Figure 6B. One can find that the hcp domain and the fcc region surrounding the growing tip are still not connected directly and are separated by the U-shaped single domain wall. As mentioned above, although there are several similar aspects of the surface reconstruction of C_{60}(111) compared to those on inorganic materials,[18,52,53] a crucial difference is that, on inorganic materials, the DLs growing in different directions never cross either themselves or each other. This difference is considered to be due to the difference between the intermolecular interaction energy and the interatomic interaction energy; the former is much smaller than the latter.

To confirm the wavelength threshold for photoinduced surface reconstruction, we also examined the effect of illumination of the surface of the C_{60} single crystals with various photon energies, e.g., 3.81, 2.78, and 2.41 eV.[54] Cracked surfaces were created when the light energy was greater than the band gap (>2.3 eV). Figure 7 shows a cracked (111) surface for a C_{60} single crystal illuminated at a photon energy of 2.41 eV. The cracks are along three [11$\bar{2}$] directions, similar to the observations of other researchers,[55,56] who have confirmed that the cracking is due to a photochemical reaction. A profile of the image (as shown in Figure 7B) indicated that the cracks extend rather deeply (more than 100 nm) into the bulk of the crystal. In contrast to super-band gap illumination, the reconstructed surface is created with sub-band gap illumination (Frenkel exciton excitation, in the range 1.5−2.0 eV), e.g., 1.96 and 1.85 eV. These experiments indicate that the Frenkel exciton excitation is responsible for the photoinduced surface reconstruction. In IR measurements of C_{60} thin film on KBr substrate,

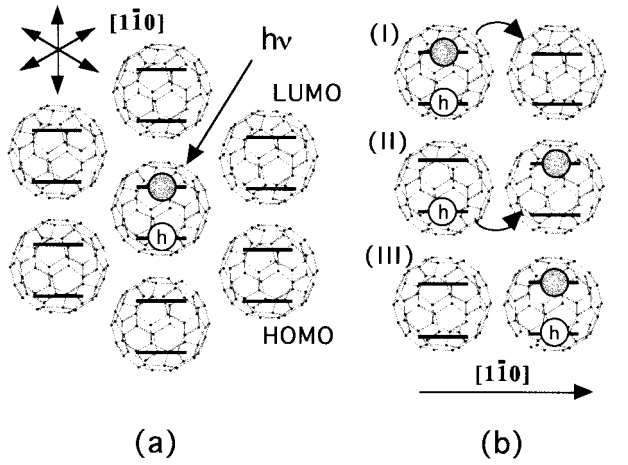

Figure 8. Molecular model of the (111) face of the C_{60} single crystal. (a) One molecule is excited, forming a Frenkel exciton. The exciton will hop to nearest-neighbor molecules along the three equivalent [1$\bar{1}$0] directions. (b) Hopping process of an exciton from an excited molecule to its nearest neighbor. (I) From the initial excitation state, the electron will hop to the LUMO of the neighboring molecule. (II) After electron hopping, the hole will follow the electron and hop to the HOMO of the neighboring molecule. (III) Finally, the whole exciton moves to the nearest-neighbor molecule. The electron−lattice coupling occurs mainly in process (II).

the IR spectrum shows no change after illumination, suggesting that no photochemical reactions[46] occur under the present illumination conditions. To determine the depth of the reconstruction, the reconstructed layers were removed in particular small areas (100 nm × 100 nm) by repeated scanning with a relatively high force (e.g., 0.5 nN) and scanning rate of 8 Hz. It was found that the dislocation occurs only to a depth of two or three layers under the present illumination conditions, even though the penetration depth of the light in the 1.5−2.0 eV range is about several micrometers into the C_{60} solid. This implies that the photoinduced reconstruction occurs less easily in the bulk than on the surface.

Upon photon absorption in the 1.5−2.0 eV range, Frenkel-type molecular excitons are induced in solid C_{60}.[47] It has been reported that these excitons may hop between nearest-neighbor molecules,[57] i.e., along the three equivalent [1$\bar{1}$0] directions on the (111) surface, as shown in Figure 8a. The hopping process between two neighboring molecules is illustrated in Figure 8b. The excitons hop in the lattice at very high rates (ca. 10^{14} Hz),[58] and it is impossible for the molecules to respond in such short times. Therefore, it is difficult to induce molecular dislocations in defect-free lattices through the hopping process of the excitons. However, the excitons may recombine at defects, undergo self-trapping, or even annihilate each other,[59,60] which may induce a strong electron−lattice coupling. Furthermore, lattice distortions have also been suggested to result from exciton relaxation.[59] Accordingly, it is considered that the type of surface reconstruction described here is induced via the relaxation of Frenkel-type excitons. The light intensity threshold value for the reconstruction further suggests that a multiexciton relaxation is necessary for the initiation of the dislocation. The initial points of DL (as shown in Figure 2) are considered to be point defects, which can act as recombination centers for the excitons. These point defects can be molecular vacancies or may involve molecular disorder on the surface of the crystal.

As for the photodriven growth process of the DLs, the growing tip of the DL may also act as a recombination center

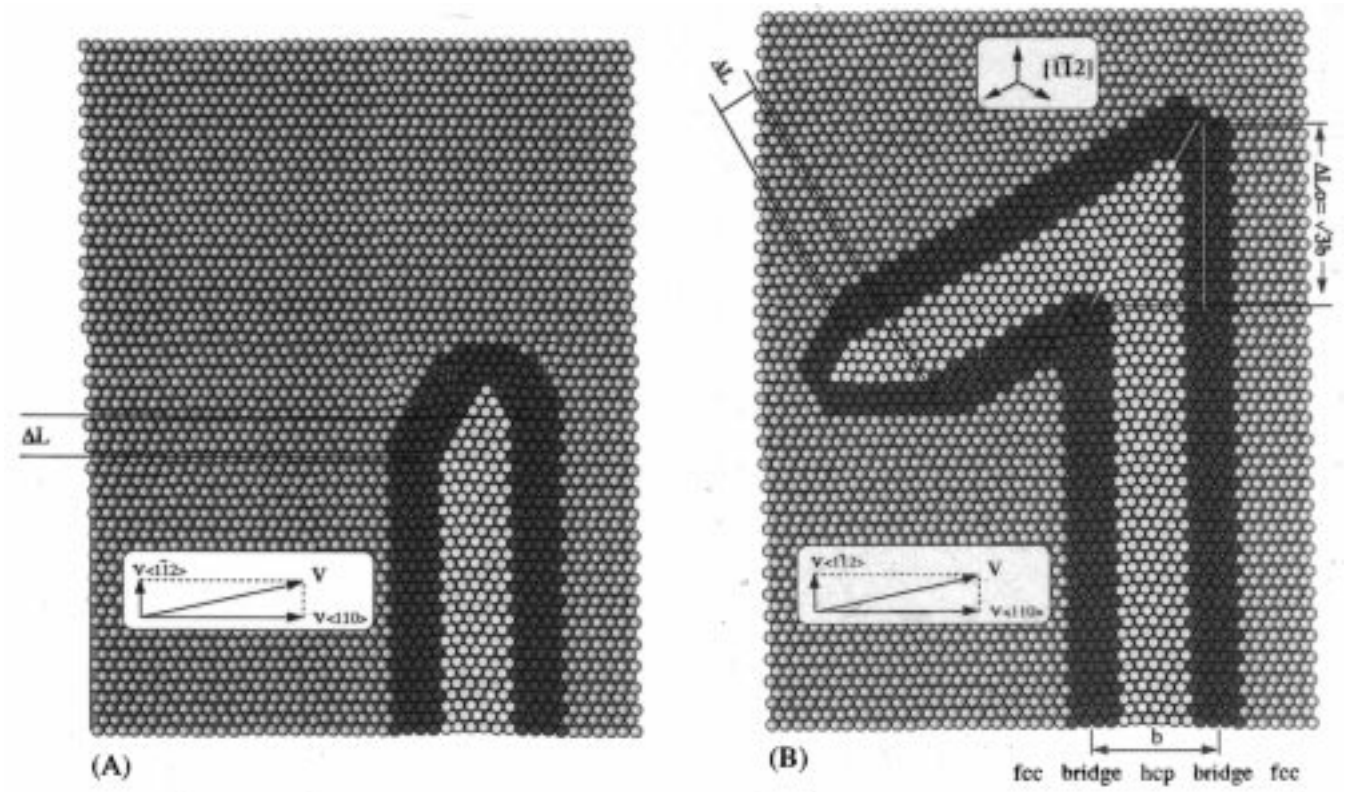

Figure 9. Proposed monolayer molecular arrangement model of an isolated dislocation line-pair growing along the ⟨11$\bar{2}$⟩ direction, (a) before and (b) after changing to a different ⟨11$\bar{2}$⟩ direction. The molecules in different sites (fcc, bridge, hcp) are represented by different colors. The insets show the relationship of the growth velocity between the ⟨1$\bar{1}$2⟩ and ⟨1$\bar{1}$0⟩ directions. The scale has been altered for clarity, so that the width of the dislocation (ridge-to-ridge, ∼30 molecules) is shown here as comprising ∼10 molecules. The asymmetric growth of the two substructures results in a length difference of the DL at the growing tip. At the turning point, ΔL_0 is equal to $\sqrt{3}b$, where b is the distance between the two substructures in the [1$\bar{1}$0] direction, i.e., perpendicular to the growth direction.

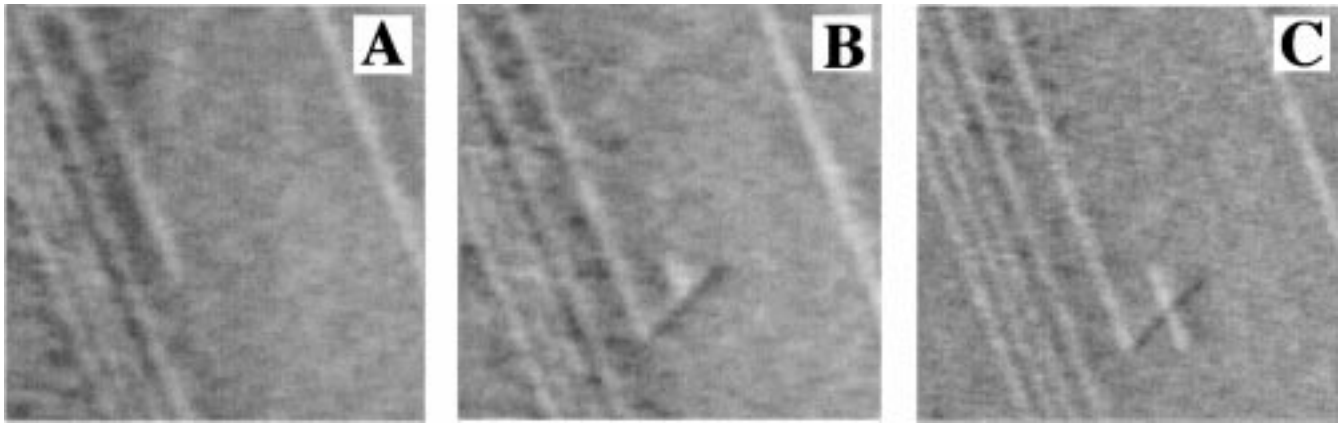

Figure 10. Successive AFM images (1.4 x 1.4 μm scale) of the photodriven triangular propagation as a DL structure (a) grows along the $\langle 11\bar{2}\rangle$ direction, (b) turns direction counterclockwise three times and returns to its original direction, and finally (c) intersects itself. The images are zoomed from low magnification images, so that the substructure-pair cannot be distinguished.

for the hopping excitons. This is because the molecular arrangement around the growing tip is highly disordered, as shown in Figure 6B. The recombination of the hopping excitons at the growing tip is considered to be the driving force for the growth of individual DLs. The number of recombining excitons at the growing tip may influence the growth rate and other dynamic features of the DLs.

We further suggest that different types of dynamic features are due to the slightly different growth rates of the two substructures in each DL. Here, a molecular arrangement model is used to discuss the dynamic behavior of the reconstruction. Figure 9 shows a monolayer molecular arrangement model of a pair of substructures in a DL (A) before and (B) after change to another $[11\bar{2}]$ growth direction. As mentioned above, the reconstruction is realized by cooperative dislocations in the $[11\bar{2}]$, $[1\bar{1}0]$, and [111] directions. The molecular dislocation in the $\langle 1\bar{1}0\rangle$ direction is energetically dictated by the fact that a relatively high energy hcp phase (compared with the fcc phase) is confined by two energetically stable fcc structures through ridged domain walls, i.e., a metastable structure. The formation of a single domain wall is energetically unstable. In fact, we can find this kind of unstable situation precisely at the U-shaped growing tip of the dislocation structure in the $[11\bar{2}]$ direction, where there is essentially a single domain wall separating the overall fcc surface from a narrow hcp strip. This instability is the main reason that the DL continues to propagate along the $\langle 11\bar{2}\rangle$ direction, as shown in Figure 9A. In the (111) plane, cooperative dislocations in the $[11\bar{2}]$ and $[1\bar{1}0]$ directions may play a major role in the dynamic reconstruction process. Figure 9B shows a proposed molecular arrangement within a DL which changes to a different $[11\bar{2}]$ direction. To realize the change in direction, the two substructures must grow with a critical length difference (in the $[11\bar{2}]$ direction) of $2\Delta L_0 = 2\sqrt{3}b$, where b is the distance between centers of the ridges in the $[1\bar{1}0]$ direction. In this case, the minimum-energy path shifts to another $[1\bar{1}0]$ direction and the DL changes to a different [112] direction, as shown in Figure 9B. The length difference ΔL is probably due to cooperative growth in the $\langle 11\bar{2}\rangle$ and $\langle 1\bar{1}0\rangle$ directions in the growing tip. It should be stressed that, since the actual scale for a dislocation in the C_{60} system involves on the order of 100 molecules across the entire structure, the magnitudes of the growth rates ($\nu_{\langle 1\bar{1}0\rangle}$) will be 2 orders of magnitude larger than those of $\nu_{\langle 1\bar{1}2\rangle}$. The relationship between the growth velocities $\nu_{\langle 1\bar{1}2\rangle}$ and $\nu_{\langle 1\bar{1}0\rangle}$ is illustrated in Figure 9. The magnitude of ΔL increases with increasing $\nu_{\langle 11\bar{2}\rangle}/\nu_{\langle 1\bar{1}0\rangle}$. This is consistent with the fact that spontaneous turning behavior was observed in the faster growing DLs. The two types of collision processes may also be due to the asymmetric growth of the two sub-structures during the collision. However, AFM observation is insufficient to confirm this. Further studies are being conducted toward theoretical simulation of surface molecular dynamics and photon−lattice interactions of the present system.

The fact that DLs exhibit such triangular traces is due to minimum-energy paths for the surface reconstruction existing only in the three equivalent $[1\bar{1}0]$ directions. Figure 10 shows successive AFM images of the photodriven triangular propagation of a DL structure (A) growing along a $\langle 11\bar{2}\rangle$ direction, (B) turning anticlockwise three times, and (C) going through itself and returning to its original direction. Finally, a regular triangular trace is presented in Figure 10C. These results also demonstrate that AFM is indeed a powerful tool with which to study the dynamic process on the surface of solids. The symmetrical growth pattern of the DLs suggests that the energy dispersion of the excitons is an anisotropic process in this highly ordered system.

In situ AFM observation of the photodriven motion of the DLs displayed unique dynamic surface reconstruction behavior. These DLs consisted of pairs of dislocation substructures. They always change direction in an anticlockwise fashion, exhibiting triangular traces when the distance between turns is short. They also show different types of collision processes, depending on the growth rate. The driving force for the reconstruction is suggested to be the relaxation of the excitons at surface defects and at the growing tip of the DL. All of these observations demonstrate that the C_{60} single crystal can serve as a useful model to probe photoinduced surface lattice dynamics of molecular crystals.

Acknowledgment. We thank Dr. T. W. Ebbesen for fruitful discussions.

References and Notes

(1) 4See: Sinha, S. K., Ed. *Ordering in Two Dimensions*; North Holland: Amsterdam, 1980, for overview.

(2) Hove, M. A. Van; Tong, S. Y. *Surface Crystallography by LEED*; Springer-Verlag, Berlin, 1979.

(3) Tanishiro, Y.; Kanamori, H.; Takayanagi, K.; Yagi, K.; Honjo, G. *Surf. Sci.* **1981**, *111*, 395.

(4) Marks, L. D.; Heine, V.; Smith, D. J. *Phys. Rev. Lett.* **1980**, *52*, 656.

(5) Wöll, Ch.; Chiang, S.; Wilson, R. J.; Lippel, H. P. *Phys. Rev. B* **1989**, *39*, 7988.

(6) Brune, H.; Röder, H.; Borrado, C.; Kern, K. *Phys. Rev. B* **1994**, *49*, 2997.

(7) Carpinelli, J. M.; Weitering, H. H.; Plummer, E. W.; Stumpf, R. *Nature* **1996**, *381*, 398.

(8) Nie, H. Y.; Mizutani, W.; Tokumoto, H. *Surf. Sci.* **1994**, *311*, L649.
(9) Wang, H.; Jing, J. T.; Chu, H.; Henriken, P. N. *J. Vac. Sci. Technol. B* **1993**, *11*, 2000.
(10) Budevski, E.; Staikov, G., Lorenz, W. J., Eds. *Electrochemical Phase Formation and Growth*; Weinheim: New York, 1996; p 9.
(11) Leibsle, F. M.; Murrary, P. W.; Francis, S. M.; Thornton, G.; Bowker, M. *Nature* **1993**, *365*, 706.
(12) Günther, C.; Vrijmoeth, J.; Hwang, R. Q.; Behm, R. J. *Phys. Rev. Lett.* **1995**, *74*, 754.
(13) Seehofer, L.; Falkenberg, G.; Daboul, D.; Johnson, R. L. *Phys. Rev. B* **1995**, *51*, 13503.
(14) Rodriguez, J. A. *Surf. Sci. Rep.* **1996**, *24*, 223, and references therein.
(15) Nagai, K.; Iyoda, T.; Fujishima, A.; Hashimoto, K. *Solid State Commun.* **1997**, *102*, 809.
(16) Koshihara, S.; Tokura, Y.; Iwasa, Y.; Koda, T. *Phys. Rev. B* **1991**, *44*, 431.
(17) Koshihara, S.; Tokura, Y.; Takeda, K.; Koda, T. *Phys. Rev. B* **1992**, *68*, 1148.
(18) Schmid, A. K.; Bartelt, N. C.; Hamilton, J. C.; Carter, C. B.; Hwang, R. Q.; *Phys. Rev. Lett.* **1997**, *78*, 3507.
(19) Morgenstern, K.; Rosenfeld, G.; Poelsema, B.; Comsa, G. *Phys. Rev. Lett.* **1995**, *74*, 2058.
(20) Pearson, C.; Borovsky, B.; Krueger, M.; Curtis, R.; Ganz, E. *Phys. Rev. Lett.* **1995**, *74*, 2710.
(21) Nakayama, K.; Jiang, L.; Iyoda, T.; Hashimoto, K.; Fujishima, A. *Jpn. J. Appl. Phys.* **1997**, *36*, 3898.
(22) Wang, R.; Hashimoto, K.; Fujishima, A.; Chikuni, M.; Kojima, E.; Kitamura, A.; Shimohigoi, M.; Watanabe, T. *Nature* **1997**, *388*, 431.
(23) Wang, R.; Hashimoto, K.; Fujishima, A.; Chikuni, M.; Kojima, E.; Kitamura, A.; Shimohigoi, M.; Watanabe, *Adv. Mater.* **1998**, *10*, 135.
(24) Tanigaki, K.; Kuroshima, S.; Ebbesen, T. W. *Thin Solid Films* **1995**, *257*, 154, and references therein.
(25) Weaver, J. H.; Poirier, D. M. *Solid State Phys.* **1994**, *48*, 1, and references therein.
(26) Kuk, Y.; Kim, D. K.; Suh. Y. D.; Park, K. H.; Noh, H. P.; Oh, S. J.; Kim, S. K. *Phys. Rev Lett.* **1993**, *70*, 1948.
(27) Li, Y. Z.; Patrin, J. C.; Chander, M.; Wever, J. H.; Chibante, L. P. F.; Smalley, R. E. *Science* **1991**, *252*, 547.
(28) Li, Y. Z.; Chander, M.; Patrin, J. C.; Wever, J. H.; Chibante, L. P. F.; Smalley, R. E. *Science* **1991**, *253*, 429.
(29) Hang, X.; Chen, D. M.; Creager, W. N. *Surf. Sci.* **1994**, *50*, 8454.
(30) Zhao, Y. B.; Poirier, D. M.; Wever, J. H. *J. Phys. Chem. Solids* **1993**, *54*, 1685.
(31) Zhao, Y. B.; Poirier, D. M.; Pechman R. J.; Wever, J. H. *Appl. Phys. Lett.*, in press.
(32) Benning, P. J.; Stepniak, F.; Wever, J. H. *Phys. Rev. B* **1993**, *48*, 9086.
(33) Kim, Y.; Jiang, L.; Iyoda, T.; Hashimoto, K.; Fujishima, A. *Surf. Sci.* **1997**, *385*, L945.
(34) Kim, Y.; Jiang, L.; Iyoda, T.; Hashimoto, K.; Fujishima, A. *Appl. Phys. Lett.* **1997**, *71*, 3489.
(35) Jiang, L.; Iyoda, T.; Tryk, D. A.; Kino, N.; Kitazawa, K.; Fujishima, A.; Hashimoto, K. *Jpn. J. Appl. Phys.* **1997**, *36*, 3903.
(36) Jiang, L.; Iyoda, T.; Kino, N.; Kitazawa, K.; Hashimoto, K.; Fujishima, A. *Surf. Sci.* **1996**, *349*, 101L.
(37) Jiang, L.; Iyoda, T.; Tryk, D. A.; Li, J.; Kitazawa, K.; Hashimoto, K.; Fujishima, A. *Surf. Sci.*, in press.
(38) Guo, Y.; Karasawa, N.; Goddard, W. A., III. *Nature* **1991**, *351*, 464.
(39) Urbach, F. *Phys. Rev.* **1953**, *92*, 1324.
(40) Mizuno, K.; Matsui, A.; Sloan, Gilbert *J. Chem. Phys.* **1989**, *131*, 423.
(41) Chiu, K. C.; Wang, J. S.; Lin, C. Y. *J. Appl. Phys.* **1996**, *79*, 1784.
(42) Hassnien, A.; Gasperic, J.; Demsar, J.; Musevic, I.; Mihailovic, D. *Appl. Phys. Lett.* **1996**, *70*, 417.
(43) Bacsa, W. S.; Lannin, J. S. *Phys. Rev. B* **1994**, *49*, 14750.
(44) Li, J.; Mitsuki, T.; Ozawa, M.; Horiuchi, H.; Kitazawa, K.; Achiba, Y. *J. Cryst. Growth* **1994**, *143*, 58.
(45) Zhou, P.; Dong, Z. H.; Rao, A. M.; Eklund, P. C. *Chem. Phys. Lett.* **1993**, *211*, 337.
(46) Rao, A. M.; Zhou, P.; Wang, K. A.; Hager, G. T.; Holden, J. M.; Wang, Y.; Lee, W. T.; Bi, X. X.; Eklund, P. C.; Cornett, D. S.; Duncan, M. A.; Amster, I. J. *Science* **1993**, *259*, 955.
(47) Lof, R. W.; Veenendaal, M. A. van; Koopmans, B.; Jonkman, H. T.; Sawatzky, G. A. *Phys. Rev. Lett.* **1992**, *68*, 3924.
(48) The growing rates were acquired before the DLs changed their directions.
(49) Campbell, D.; Peyrard, M.; Sodano, P. *Physica D* **1986**, *19*, 165.
(50) EI-Baanouny, M.; Burdick, S.; Martini, K. M.; Stancioff, P. *Phys. Rev. Lett.* **1987**, *58*, 27.
(51) Krakow, W.; Rivera, N. M.; Roy, R. A.; Ruff, R. S.; Cuomo, J. J. *J. Mater. Res.* **1992**, *7*, 784.
(52) Bott, M.; Hohage, M.; Michely, T.; Comsa, G. *Phys. Rev. Lett.* **1993**, *70*, 1489.
(53) Barth, J. V.; Barth, H. G.; Behm, Ertl, R. J. *Phys. Rev. B* **1990**, *42*, 9307.
(54) Kim, Y.; Jiang, L.; Iyoda, T.; Li, J.; Kitazawa, K.; Hashimoto, K.; Fujishima, A. *J. Appl. Phys. A* **1998**, *66*, S763.
(55) Verherijien, M. A.; Meekes, H.; Meijer, G.; Raas, E.; Bennema, P. *Chem. Phys. Lett.* **1992**, *191*, 339.
(56) Haluska, M.; Kuzmany, H.; Vybornov, M.; Rogl, P.; Fejdi, P. *Appl. Phys.* **1993**, *A56*, 161.
(57) Janner, A.-M.; Eder, R.; Koopmans, B.; Jonkman, H. T.; Sawatzky, G. A. *Phys. Rev. B* **1995**, *52*, 17158, and references therein.
(58) Brühwiler, P. A.; Maxwell, A. J.; Rudolf, P.; Gutleben, C. D.; Wästberg, B.; Martensson, N. *Phys. Rev. Lett.* **1993**, *71*, 3721.
(59) Muccini, M. *Synth. Met.* **1996**, *83*, 213.
(60) Lee, C. H.; Yu, G.; Moses, D.; Srdanov, V. I.; Wei, X.; Vardeny, Z. V. *Phys. Rev. B* **1993**, *48*, 8506.